Precision force and position control of ionic polymer–metal composite

N Bhat and **W-J Kim***
Department of Mechanical Engineering, Texas A&M University, Texas, USA

Abstract: In this paper, model-based precision force and position control of an ionic polymer metal composite (IPMC) is presented. A 23.8 mm × 3.4 mm × 0.16 mm IPMC strip was used as an actuator in a cantilever configuration. Open-loop force and position responses of an IPMC are not repeatable, and hence closed-loop precision control is of critical importance to ensure proper functioning, repeatability and reliability. After feedback controllers were designed and implemented with empirically obtained fourth-order plant transfer functions, the overshoot decreased from 460 to 2.8 per cent and the settling time was reduced from 37.5 to 3.22 s in force control. In position control the overshoot decreased from 333 to 20.3 per cent and the settling time was reduced from 21.5 to 2.56 s. Microscale precision force and position control capabilities of the IPMC actuator were also demonstrated experimentally. An 8 μN force resolution was achieved with a force noise of 0.5 μN r.m.s., and the position resolution was 6 μm with a position noise of 2.5 μm r.m.s. The maximum force and tip displacement achieved with the IPMC actuator under closed-loop control were 2 mN and 5 mm respectively. The IPMC actuator could follow various commanded force and position trajectories such as sinusoidal and trapezoidal position profiles, and a velocity profile with a 3 mm/s maximum velocity. A novel hybrid force and position control strategy demonstrated its utility in practical micromanipulation applications where the actuator force must be limited to prevent damaging micro-objects. High-precision control of the IPMC at low force level proved its potential for micromanufacturing and micromanipulation applications such as robotic and biomedical microgrippers.

Keywords: ionic polymer–metal composite, microscale force control, microscale position control, smart material actuator, hybrid control

NOTATION

a, b, c, d	curve-fitting parameters for modelling (s^{-1})
C_1	open-loop steady state force constant (N)
C_2	open-loop steady state position constant (m)
d_a	actual tip displacement sensed by the laser distance sensor in the hybrid position and force control (m)
d_r	reference displacement command in the hybrid control (m)
f_a	actual force sensed by the precision load cell in the hybrid control (N)
f_p	threshold force in the hybrid control (N)
f_r	reference force command in the hybrid control (N)
V	voltage applied to the IPMC strip in open loop (V)
y_1, y_2, y_3	curve-fitting parameters for modelling (N or m)

The MS was received on 3 November 2003 and was accepted after revision for publication on 2 June 2004.
** Corresponding author: Department of Mechanical Engineering, Texas A&M University, College Station, TX 77843-3123, USA. E-mail: wjkim@mengr.tamu.edu*

1 INTRODUCTION

Electroactive polymers, which respond to external electrical stimulation with significant shape and size change, can be classified into two major categories based on their activation mechanisms—electronic and ionic [**1**]. Electronic polymers include electrostrictive, electrostatic, piezoelectric and ferroelectric polymers that require high activation voltage. The position of the electronic polymer based actuators can be well controlled as they

mi00001003 04-08-04 16:40:13 Rev 14.05
The Charlesworth Group, Huddersfield 01484 517077

can hold the induced displacement under the application of a d.c. voltage. Ionic electroactive materials include ionic gels, ionic polymer metal composites, conducting polymers and carbon nanotubes. The ionic polymer based actuators require an activation voltage of only 1–5 V, but it is difficult to maintain a constant position under d.c. activation since it acts as a leaky capacitor [**1**].

An ionic polymer–metal composite (IPMC) as an ionic electroactive polymer consists of a base polymer coated with electrodes made up of highly conducting pure metals such as gold. There are two types of base polymer that can be used to form an IPMC: Nafion® (manufactured by DuPont) and Flemion® (manufactured by Asahi Glass) [**1**]. Figure 1 shows the chemical structure of the Nafion-based IPMC [**2**].

An IPMC contains an ion-exchange membrane and requires a solvent such as water to facilitate ion migration. The lithium ion is the mobile cation M^+ in Fig. 1 in the IPMC strip used in this research. On the application of positive voltage across a fully hydrated IPMC strip, mobile ion migration takes place from the anode towards the cathode. Water molecules travel with the mobile ions simultaneously. This net migration of lithium ions and water molecules results in a bending of the IPMC strip. Shahinpoor [**3**], Oguru *et al.* [**4**] and Sadeghipour *et al.* [**5**] discovered this electroactive behaviour of IPMCs in 1992 for the first time. Although this paper focuses on the usage of an IPMC as an actuator, IPMCs can also be used as force sensors. Under application of an external force, when the IPMC strip bends, mobile cations shift owing to the presence of a stress gradient across the thickness, and this shifting of the mobile cations can be translated into a voltage gradient measurable across the thickness of the IPMC strip. This output voltage can be calibrated into the force applied [**2**].

A smart actuator based on an IPMC has many advantages:

1. It requires a low activation voltage (less than 5 V).
2. It produces a relatively large displacement compared with electronic polymers.
3. It can operate well in a wet environment.
4. It can be made with a single moving part in the form of a small strip.

Table 1 presents a comparison between an IPMC and other well-known smart materials. The stress generated by an IPMC is small compared with that generated by a shape memory alloy (SMA) and lead zirconium titanate (PZT). The efficiency of an IPMC is higher than that of an SMA and almost the same as that of PZT. Therefore, an IPMC has potential in low-mass, large-displacement actuation and other applications.

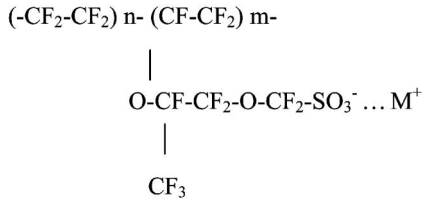

Fig. 1 Chemical structure of the IPMC

Table 1 Comparison of an IPMC with other smart materials [**6**]

Smart materials	Strain (%)	Stress (MPa)	Efficiency (%)
Piezoelectric	0.09	35	>30
SMA	>5	>200	>3
Magnetostrictive	0.2	70	<30
Electrostatic	>10	0.04	>20
IPMC	>40	0.3	>30

Konyo *et al.* used IPMC actuators to produce an artificial tactile feel display to provide human operators with the required stimuli [**7**]. Bar-Cohen *et al.* developed an IPMC-based planetary dust wiper to remove dust particles from the surface of a Nanorover [**8**]. Bar-Cohen *et al.* designed and constructed a miniature robotic arm [**9**]. An IPMC can be a good candidate to substitute for human muscles owing to its flexibility, softness and large displacement [**10**]. An IPMC-based actuator is also well suited in micromanipulation and microfabrication applications for microassembly of small parts. Lumia and Shahinpoor designed a microgripper that used both actuation and sensing capabilities of an IPMC [**11**]. Kim and Bhat conceived of an idea of using IPMC strips as fingers for a microgripper system [**12**].

The open-loop response of an IPMC to an external electrical stimulation is characterized by fast recoiling towards the anode followed by bending towards the cathode and finally slow return to its initial status. It cannot maintain a steady position or force upon the application of a d.c. voltage in open-loop operation owing to the complicated electrochemical reaction in the ionic polymer material [**1**]. In addition, its open-loop overshoot is large, of the order of 300–400 per cent, while the open-loop settling time is long, of the order of 10–30 s. Thus, it is difficult to use an IPMC as key components in an actuator without feedback control for applications such as robotic and biomedical manipulators, which should rapidly move from one specified position to another and maintain the commanded reference position. Hence, closed-loop precision position control is of critical importance to ensure proper functioning, repeatability and reliability.

Precision force control has equal importance in many future applications of IPMCs. Consider a microgripper system having IPMC strips as the fingers. In the micro-domain the force required to grip a micro-object is small owing to the dominance of adhesion forces compared with the gravitational force. The Van der Waals force is a significant constituent of the adhesion forces experienced in micromanipulation. As the Van der Waals force

is greatly influenced by the applied force, controlling the force exerted by an IPMC is crucial to limit the adhesion forces [**13**]. On the other hand, excessive force may damage the micro-object. Thus microscale precision control of force produced by an IPMC is crucial in next-generation micromanipulation and micromanufacuring systems with IPMC actuators.

In the following section, the IPMC experimental set-up is described. Section 3 discusses modelling and both precision force and position control based on lead-lag compensation. Key experimental performance characteristics such as microscale force and position control, dynamic force and position ranges, actuator speed and ability to track various commanded force and position trajectories are given in section 4. A novel hybrid force and position control strategy presented in section 5 demonstrates its utility in practical micromanipulation applications where the actuator force must be limited to prevent damaging micro-objects.

2 IPMC SPECIFICATIONS AND EXPERIMENTAL SET-UP

Figure 2 shows the schematic of the experimental set-up used to conduct open-loop and closed-loop force experiments. The dimensions of the IPMC strip used in this research are 23.8 mm × 3.4 mm × 0.16 mm. A clamp as seen in the figure purchased from McMaster-Carr was modified by attaching two 11.43 mm × 4.28 mm × 1.27 mm copper electrodes (99.9 per cent pure copper foil from Alfa Aesar). Two holes were drilled on the jaws of the clamp behind the copper electrodes to solder wires to them. A precision load cell (model GM2 from SCAIME) with a force resolution of 900 nN was used for force sensing. It was mounted on the platform such that the tip of the IPMC strip would touch the load cell. The output signal of the load cell was very small and thus was amplified using a signal amplifier (CMJ-CEB series from SCAIME). A differential instrument preamplifier (model ADA 400 from Tektronix) was used to amplify the signal further and reject noise. The output signal from the differential preamplifier was fed to a 16 bit analogue-to-digital (A/D) converter on a digital signal processor (DSP) controller board (model DS1102 from dSPACE). The controller board has a Texas Instruments TMS320C31 floating-point DSP.

The experimental set-up used to conduct the open-loop and closed-loop positioning experiment is very similar to that for force experiments; the only difference is the use of a laser distance sensor (model OADM 20144/404790 from Baumer Electric) to sense the IPMC tip position. This laser distance sensor has a resolution of 5 μm, and its operation range is 10 mm with a stand-off of 15 mm. Its response time is specified to be less than 10 ms. It works on the principle of optical triangulation and can detect the tip displacement up to a bending angle of 30° [**14**]. The IPMC strip acts as a bending actuator in a cantilever configuration. The laser distance sensor was placed so that the laser beam was incident and reflected on the free end of the IPMC strip. It should be noted that the measured tip displacement does not represent the linear movement of the IPMC strip but rather the deflection of its free end which can be calibrated to a bending angle. Figure 3 is a photograph of the experimental set-up used for closed-loop force and position control experiments.

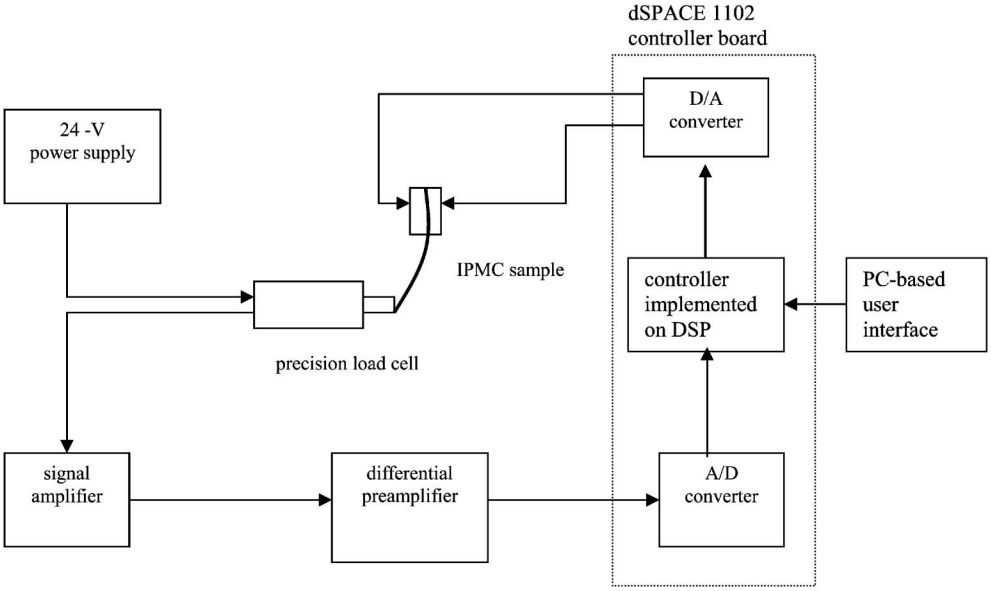

Fig. 2 Schematic of the experimental set-up used to conduct open-loop and closed-loop force experiments

mi00001003 04-08-04 16:40:13 Rev 14.05
The Charlesworth Group, Huddersfield 01484 517077

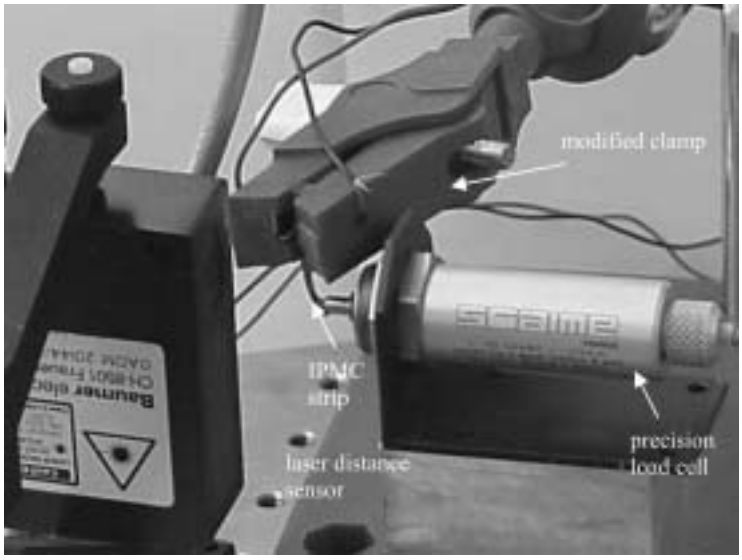

Fig. 3 Photograph of the experimental set up (1:1 scale; the screw holes of the vibration isolation table shown in the lower middle part of the figure are 25.4 mm apart). The IPMC strip touching the precision load cell is held in the modified clamp. The laser distance sensor is seen to the left of the IPMC strip

3 MODELLING AND CONTROL SYSTEM DESIGN

3.1 Force controller development

Previous research on IPMC control focused on position control using a linear quadratic regulator (LQR) and proportional integral and derivative (PID) and impedance control schemes [**15**–**17**]. Model-based loop-shaping control systems were developed to control the force and position of the present IPMC actuator. To design a force controller, a transfer function from the input voltage and the force output of the IPMC actuator should be derived [**18**]. To measure the force there should be a physical contact between the load cell and the IPMC strip. The presence of a water layer on the IPMC strip creates wet stiction between the strip and the load cell tip. Owing to this stiction, some force exists that should be compensated for.

A 1.2 V step input was applied to the IPMC actuator for a period of 50 s with a sampling rate of 250 Hz, and its open-loop step response was obtained (Fig. 4a). A rise time of 0.0381 s, a settling time of 37.5 s and an overshoot of 460 per cent characterized the open-loop step response. Hence, the present control objectives were to reduce the large settling time and overshoot and eliminate the steady state error.

For the model development, a Matlab command for least-squares curve fitting LSQCURVEFIT was used [**19**]. As the step response showed an exponential decay after its peak value, the data obtained were fitted to be

$$y(t) = y_1 \, \mathrm{e}^{-at} + y_2 \, \mathrm{e}^{-bt} + C_1 \qquad (1)$$

where C_1 is the open-loop steady state force constant found to be 1.7×10^{-4} N as in Fig. 4a. By using LSQCURVEFIT, the parameters y_1, y_2, a and b were estimated to be

$$y_1 = 0.0007 \text{ N}$$

$$y_2 = 0.0001 \text{ N}$$

$$a = 0.0836 \text{ s}^{-1}$$

$$b = 0.0836 \text{ s}^{-1}$$

The squared residual norm for this curve fit was 3.8854×10^{-5} N^2.

To decrease the squared residual norm further, a fourth-order empirical model was developed:

$$y(t) = y_1 \, \mathrm{e}^{-at} + y_2 \, \mathrm{e}^{-bt} - y_3(\mathrm{e}^{-ct} - \mathrm{e}^{-dt}) + C_1 \qquad (2)$$

Using LSQCURVEFIT once again, the parameters y_1, y_2, y_3, a, b, c and d were estimated to be

$$y_1 = 0.0238 \text{ N}$$

$$y_2 = -0.0237 \text{ N}$$

$$y_3 = 0.0030\text{i N}$$

$$a = 0.1823 \text{ s}^{-1}$$

$$b = 0.1921 \text{ s}^{-1}$$

$$c = 1.1330 - 0.2369\text{i s}^{-1}$$

$$d = 1.1330 + 0.2369\text{i s}^{-1}$$

The squared residual norm in this case was significantly decreased by 66.52 per cent to 1.3008×10^{-5} N^2, and this model was used for controller development. Taking the Laplace transformation of the output and input

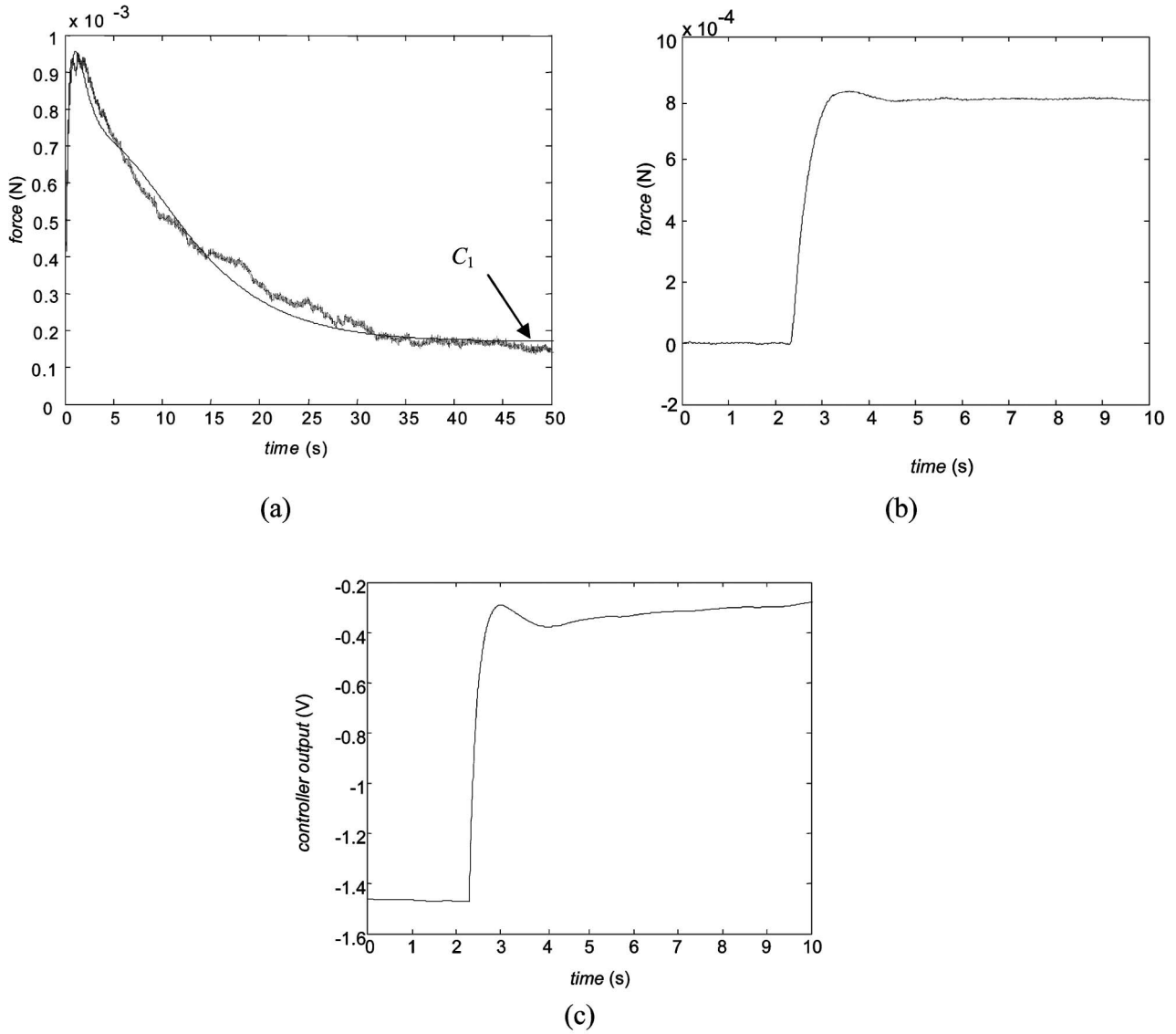

Fig. 4 (a) Actual and curve-fitted open-loop force responses of the IPMC actuator to a 1.2 V step input, (b) the closed-loop force response to a 0.8 mN step input with the digital lead-lag compensator [equation (6)] implemented and (c) the voltage output profile generated by the controller to achieve the closed-loop force response shown in (b)

equations yields

$$Y(s) = \frac{y_1}{s+a} + \frac{y_2}{s+b} - y_3\left(\frac{1}{s+c} - \frac{1}{s+d}\right) + \frac{C_1}{s} \quad (3)$$

$$U(s) = \frac{V}{s} \quad (4)$$

where V is the 1.2 V input step voltage. After substituting the values of y_1, y_2, y_3, a, b, c, and d, the transfer function from the input voltage to the output force of the IPMC actuator was found to be

$$\frac{Y(s)}{U(s)} = 10^{-6}\frac{334.2s^4 + 2503s^3 + 1726s^2 + 501.7s + 7.973}{1.2s^4 + 3.168s^3 + 2.668s^2 + 0.697s + 0.05628} \quad (5)$$

The Matlab tool *rltool* was used extensively for the controller design. Several control design iterations were performed before the controller presented in this section was finalized. Based on the developed model the poles were placed and simulations were performed on the basis of the model. If the simulation results were satisfactory, the controller was implemented on the actual system and the closed-loop performance was analysed. Initially, only a lag compensator was implemented to minimize the steady state error, and experiments were performed using that compensator. However, the damping was inadequate in the case of force control, and this lag compensator did not meet the requirements of settling time and overshoot. Hence, to increase the damping and to enhance the phase margin of the system, a lead compensator was

mi00001003 04-08-04 16:40:13 Rev 14.05
The Charlesworth Group, Huddersfield 01484 517077

added to the closed-loop system. Eventually, to eliminate the steady state error, a free pole was placed at the origin. The following digital lead-lag compensator with a sampling frequency of 250 Hz was designed and implemented to achieve the control objectives.

$$G_C(z) = 90.9\frac{(z-0.605)(z-0.977)}{(z-1)(z-0.955)} \tag{6}$$

This control system has a phase margin of 92.1° at a crossover frequency of 1.81 Hz. Figure 4b shows the closed-loop response to a 0.8 mN step force input with this lead-lag compensator. The settling time was reduced to 3.22 s, and the overshoot decreased to 2.8 per cent. This controller effectively reduced the noise components beyond the crossover frequency by more than a factor of 10 (cf. the open-loop force response shown in Fig. 4a). The voltage input applied to the IPMC strip was limited to ± 2 V to prevent breakdown in the ionic polymer base, which also limited the voltage swing of the controller output. The load cell used was very sensitive to force variations. A certain initial residual force had been developed in this contact-type load cell in contact with the IPMC strip even before the controller was started. This residual force was offset in the control loop by subtracting it from the actual sensor reading. Hence, the initial control voltage output in Fig. 4c from $t = 0$ s to $t = 2.3$ s was required to cancel the residual force before the step command was given. The controller output drift shown in Fig. 4c might result from the behaviour of the IPMC as a leaky parallel-plate capacitor [**1**]. Hence, even after reaching the commanded force, the controller should generate a changing voltage input to the actuator to maintain a steady force.

3.2 Position controller development

An IPMC transfer function was also derived from the voltage input to the tip displacement. Similar to the force model presented in the previous section, an empirical model was obtained on the basis of the experimental open-loop position response to a 1.2 V step input voltage as shown in Fig. 5a. The step response data were fitted to be

$$y(t) = y_1\,\mathrm{e}^{-at} + y_2\,\mathrm{e}^{-bt} - y_3(\mathrm{e}^{-ct} - \mathrm{e}^{-dt}) + C_2 \tag{7}$$

where C_2 is the open-loop steady state position constant, observed to be around 0.3 mm. The values of y_1, y_2, y_3, a, b, c and d were obtained by the least-squares curve-fitting methodology. The transfer function from the input voltage and the output tip displacement of the IPMC strip was found to be

$$\frac{Y(s)}{U(s)} = \frac{0.1617s^4 + 10.41s^3 + 133.2s^2 + 471.3s + 16.06}{1.2s^4 + 25.06s^3 + 177.4s^2 + 426.2s + 64.24} \tag{8}$$

Figure 5a shows that the simulated response with this model matched the actual response well. However, the open-loop position response showed an overshoot of nearly 333 per cent and a settling time of 21.5 s. The following digital lead-lag compensator was designed and implemented at a sampling frequency of 250 Hz to satisfy the control objectives of decreasing the settling time and overshoot, and eliminating the steady state error. A free pole was placed at the origin to decrease the steady state error

$$G_c(z) = 0.088\frac{(z-0.716)(z-0.946)}{(z-1)(z-0.869)} \tag{9}$$

This control system has a phase margin of 71.7° at a crossover frequency of 2.2 Hz. Figure 5b shows the closed-loop response to a 1 mm step input. The overshoot decreased to 20.3 per cent and the settling time was reduced to 2.56 s. Figure 5c shows the control voltage generated by the controller in this closed-loop position response. Possibly owing to the charges initially stored in the IPMC, the IPMC strip might bend backwards momentarily and go out of the sensing range when the step command is given. To avoid this difficulty, the IPMC strip was initially placed at a non-zero position. The initial position reading was compensated for in the control loop by subtracting it from the actual sensor reading. Hence, an initial control voltage output in Fig. 5c from $t = 0$ s to $t = 1.2$ s was required to cancel the initial position offset before the step command was given.

4 HIGH-PRECISION EXPERIMENTAL RESULTS UNDER CLOSED-LOOP CONTROL

To use an IPMC in next-generation micro- or nano-manipulation devices, high-precision control of the IPMC force and tip displacement is of primary importance. Figure 6a shows commanded and actual 8 μN step responses obtained with the IPMC strip under closed-loop force control. The force resolution is therefore better than 8 μN with a force noise of 0.5 μN r.m.s. Figure 6b shows commanded and actual 6 μm step responses under closed-loop position control; the position resolution is better than 6 μm with a position noise of 2.5 μm r.m.s. Thus, these step responses demonstrated the microscale force and position control capabilities of an IPMC actuator in a cantilever configuration.

To determine the dynamic force and position ranges of this IPMC actuator, maximum achievable force and tip displacement under closed-loop control were generated. Figures 6c and d show the closed-loop responses of the IPMC strip to 2 mN and 5 mm step inputs. Thus, the dynamic force and displacement ranges of the IPMC actuator are at least 8 μN to 2 mN and 6 μm to 5 mm

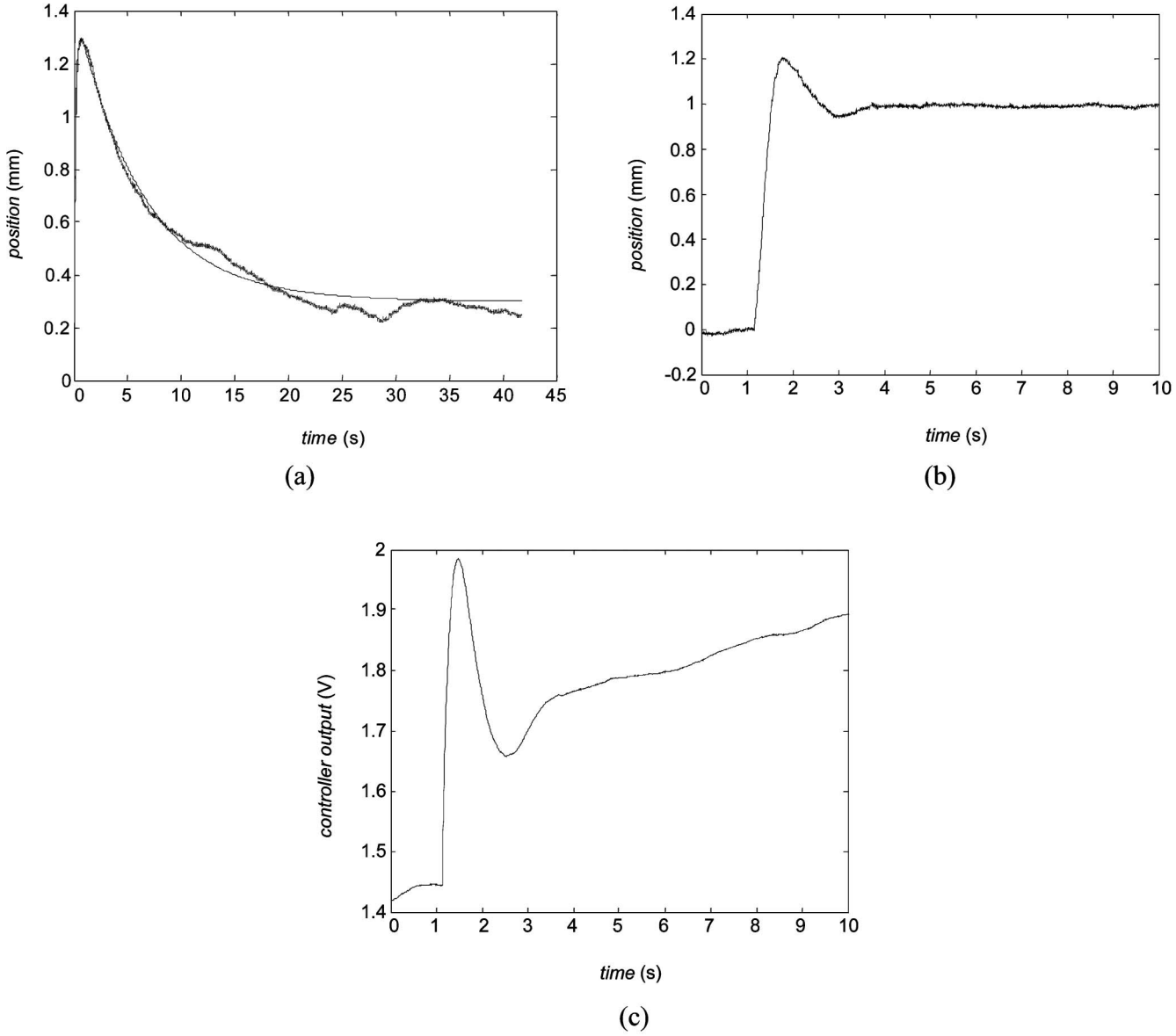

Fig. 5 (a) Actual and curve-fitted open-loop position responses of the IPMC actuator to a step input of 1.2 V, (b) the closed-loop position response to a 1 mm step input with the digital lead-lag compensator [equation (9)] implemented and (c) the voltage output profile generated by the controller to achieve the closed-loop position response shown in (b)

respectively. Although the maximum force obtained closed-loop control is small compared with that of some other smart material actuators, this wide dynamic range is suitable for low-mass, large-displacement actuation applications. The maximum achievable displacement was limited by the maximum angle the IPMC could bend before it went out of the sensing range of the laser distance sensor. The maximum achievable force was limited by the saturation voltage which limited the voltage swing of the controller. Within the sensing ranges, the closed-loop system was stable.

This IPMC actuator can also follow various high-precision force and position trajectories, as shown in Fig. 7. As expected, the actuator followed well the commanded input profiles with the driving frequencies less than the crossover frequency. To determine the maximum velocity that the IPMC actuator could generate under closed-loop control, trapezoidal velocity profiles were generated using a combination of ramps in Simulink. As the laser distance sensor gives the position feedback, the velocity profile generated was passed through an integrator block in Simulink, and the closed-loop response of the IPMC tip displacement was compared with the commanded position profile. Figure 8 compares the actual and commanded position trajectories. The IPMC strip responded well to the 3 mm/s commanded velocity.

mi00001003 04-08-04 16:40:13 Rev 14.05
The Charlesworth Group, Huddersfield 01484 517077

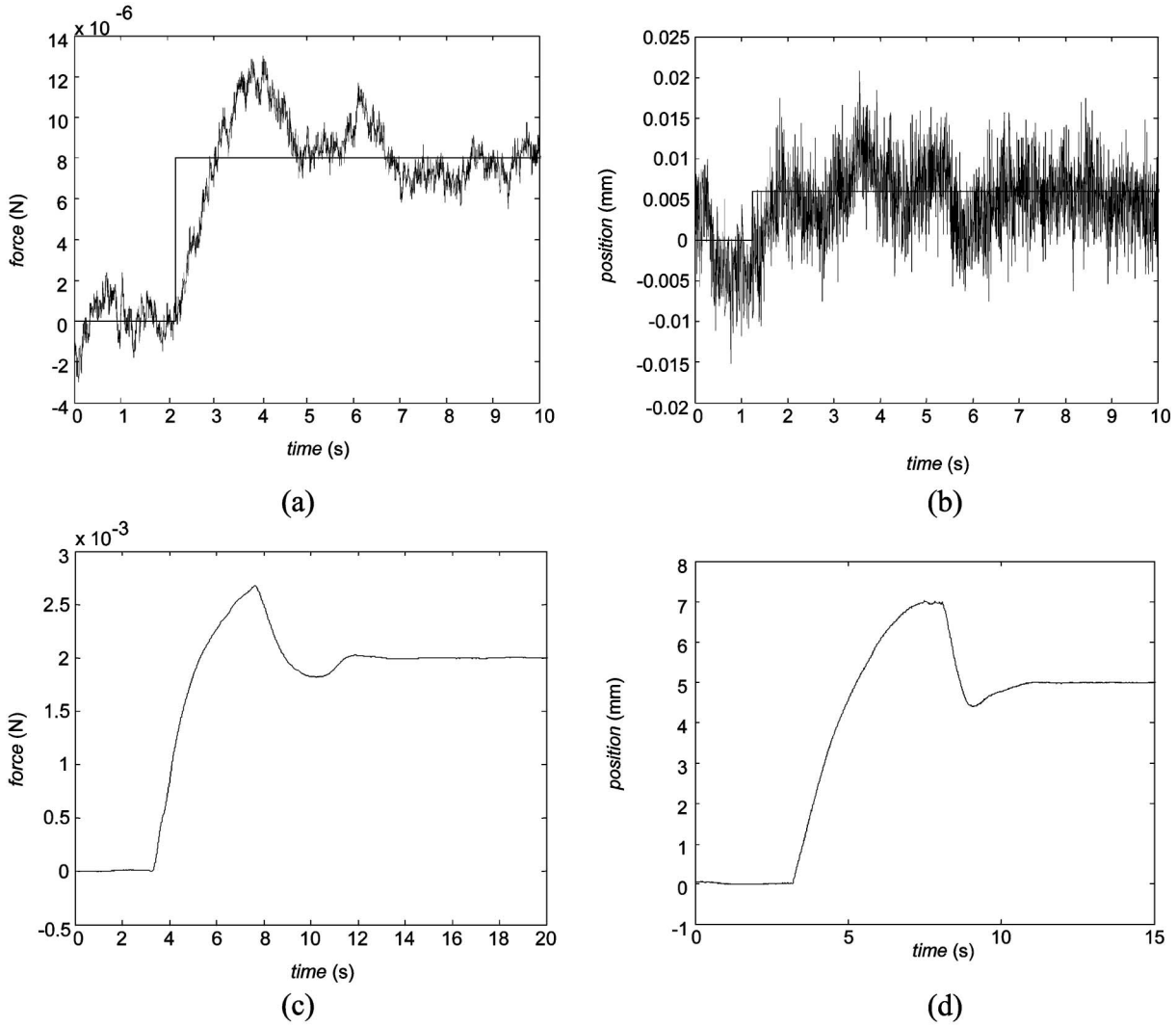

Fig. 6 (a) Actual and commanded 8 μN step responses under precision closed-loop force control, (b) the actual and commanded 6 μm step responses under precision closed-loop position control, (c) the 2 mN step response under closed-loop force control and (d) the 5 mm step response under closed-loop position control. The solid lines in (a) and (b) represent the corresponding reference command profiles

5 HYBRID POSITION AND FORCE CONTROL

One promising application of an IPMC is a three-finger robotic microgripper with two fingers used as actuators and the third finger as a force sensor generating a voltage signal proportional to the bending reaction force of the IPCM. Consider the task of manipulating a delicate micro-object with this gripper when the fingers are under precision position control. To accomplish this task without vision feedback, the gripper fingers are to be commanded to move a specified displacement, d_r, so that they close around the object and grab it. If the fingers come in contact with the micro-object after the fingers move only d_a (where $d_a < d_r$), traversing the whole commanded displacement d_r may damage the micro-object owing to the application of excessive force generated by the fingers. If the overall control action is turned off after the initial contact, however, the IPMC fingers will resume their original positions and the gripping task will fail. One possible way of overcoming this difficulty is to use a hybrid position and force control scheme. In this hybrid control, the third finger senses the contact force, and the force controller maintains the force at a reference value sufficient to grip the micro-object without damaging it.

Figure 9 shows a control loop to implement this proposed hybrid position and force control on the present single-finger IPMC actuator. In this figure, f_a and d_a are the actual force and tip displacement sensed by the precision load cell and the laser distance sensor respectively, which are employed together in this hybrid control. From the beginning, both the controllers are operational and each controller output is updated using corresponding sensor measurement. When f_a is less than the

mi00001003 04-08-04 16:40:13 Rev 14.05
The Charlesworth Group, Huddersfield 01484 517077

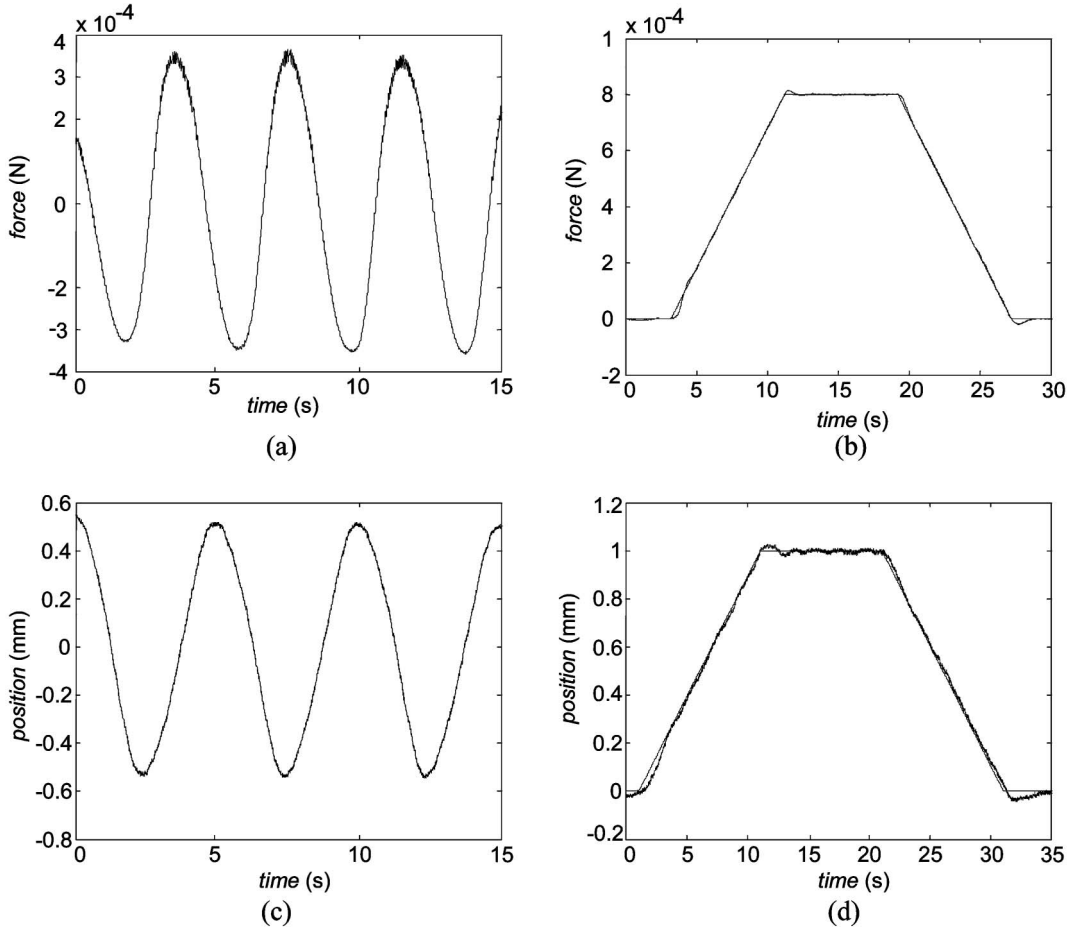

Fig. 7 Closed-loop responses to (a) a sinusoidal force command with an amplitude of 300 μN and a frequency of 0.25 Hz, (b) a trapezoidal force profile, (c) a sinusoidal position command with an amplitude of 0.5 mm and a frequency of 0.25 Hz and (d) a trapezoidal position profile. The solid lines in (b) and (d) represent the corresponding reference command profiles

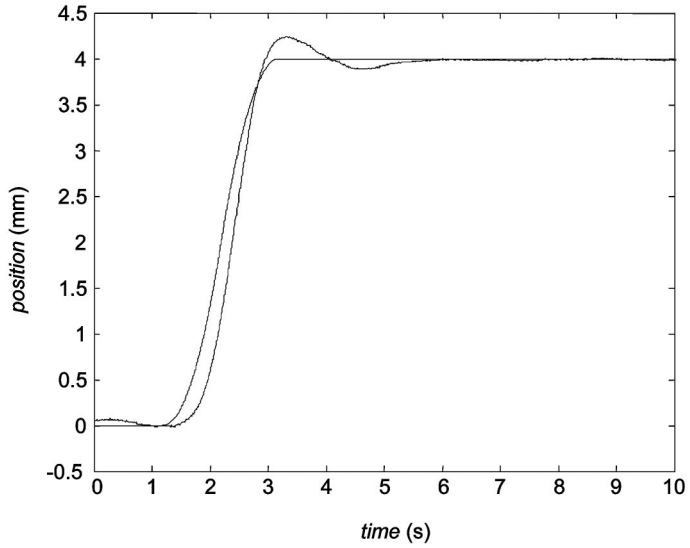

Fig. 8 Actual and commanded position trajectories obtained from a trapezoidal velocity profile with a 3 mm/s maximum velocity

mi00001003 04-08-04 16:40:13 Rev 14.05
The Charlesworth Group, Huddersfield 01484 517077

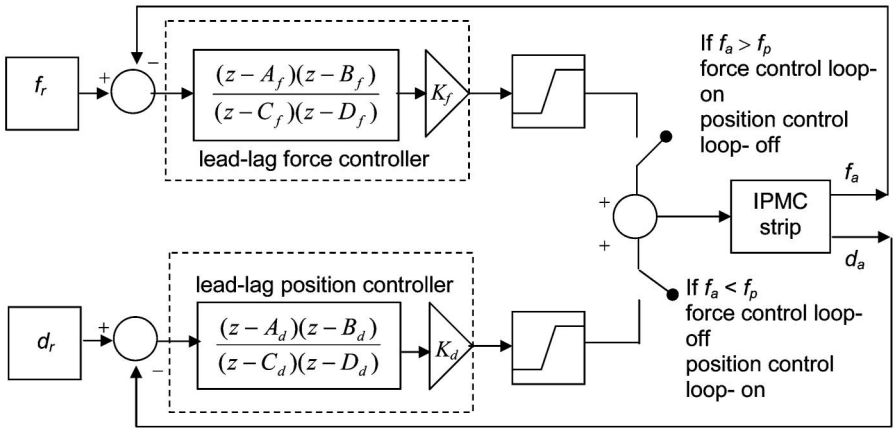

Fig. 9 Control loop to implement the hybrid position and force control scheme. The ± 2 V saturation blocks before the IPMC strip prevent damage

threshold force f_p at the beginning of the gripping operation, the position control loop is switched on. If f_a should exceed f_p, the force control would take over to maintain the force at the reference value of f_r with the position control switched off. Hence, it is only the position control or the force control that is switched on at any given instant of time with a threshold algorithm, although both controllers are active all the time.

Figure 10 shows the actual position and force responses generated by the present IPMC actuator under the hybrid position and force control. Here, d_r, f_p and f_r were set to be 0.8 mm, 1.2 mN and 1.4 mN respectively. Initially, the IPMC actuator followed the commanded position profile. When the sensed force exceeded f_p at $t = 8.2$ s, the position controller was switched off and the force controller took over. While the position controller was in charge, however, the integrator present in the force controller accumulated a significant error signal. In the hybrid control scheme, both the force and the position controllers are always operational. When the position controller is used in the loop, the force controller is on but its output signal is not sent to the IPMC strip. Hence, the error in force keeps increasing as force regulation does not take place. After the force control is brought back to the control loop, this error accumulation may cause the controller to output very high voltages exceeding the saturation limit and force the actuator to saturate. This phenomenon, in which error accumulation takes place owing to the integration effect, is called integrator wind-up.

As a result of this wind-up effect, the force controller output was saturated at 2 V when it was switched on at $t = 8.2$ s. Between $t = 8.2$ s and $t = 24$ s the force exceeded f_p and slowly approached f_r, and the control system came out of saturation. Thereafter, the IPMC actuator successfully maintained the force at its reference value of 1.4 mN. This experimental result validated the proposed hybrid position and force control scheme for realistic robotic or biomedical micromanipulation applications. This hybrid control scheme can be easily extended to a three-finger microgripper system.

6 CONCLUSIONS

An actuator based on an IPMC shows significant potential in low-mass, large-displacement applications and has many advantages:

1. It operates at low drive voltage.
2. It produces large displacement.
3. It can operate very well in a wet environment.
4. It can be made with a single moving part in the form of a small strip.

An IPMC can generate low-level, high-resolution force, which is ideal for microdevice applications such as microgrippers.

In this research an IPMC actuator was used in a cantilever configuration. An open-loop force response of an IPMC strip to a 1.2 V step input showed an overshoot of 460 per cent and a settling time of 37.5 s. The open-loop tip displacement of the IPMC strip to a 1.2 V step input showed an overshoot of 333 per cent and a settling time of 21.5 s. It was observed that both the open-loop force and position responses were not repeatable owing to the complicated electrochemical reaction in the ionic-polymer material.

Fourth-order empirical transfer functions from the voltage input to the force and position outputs were derived using a least-squares curve-fitting methodology. The control objectives were to reduce the settling time and percentage overshoot and eliminate the steady state error. The phase margin of the force controller was 92.1° and the crossover frequency was 1.8 Hz. After implementing this force controller on the IPMC actuator, the overshoot was reduced to 2.8 per cent and the settling time

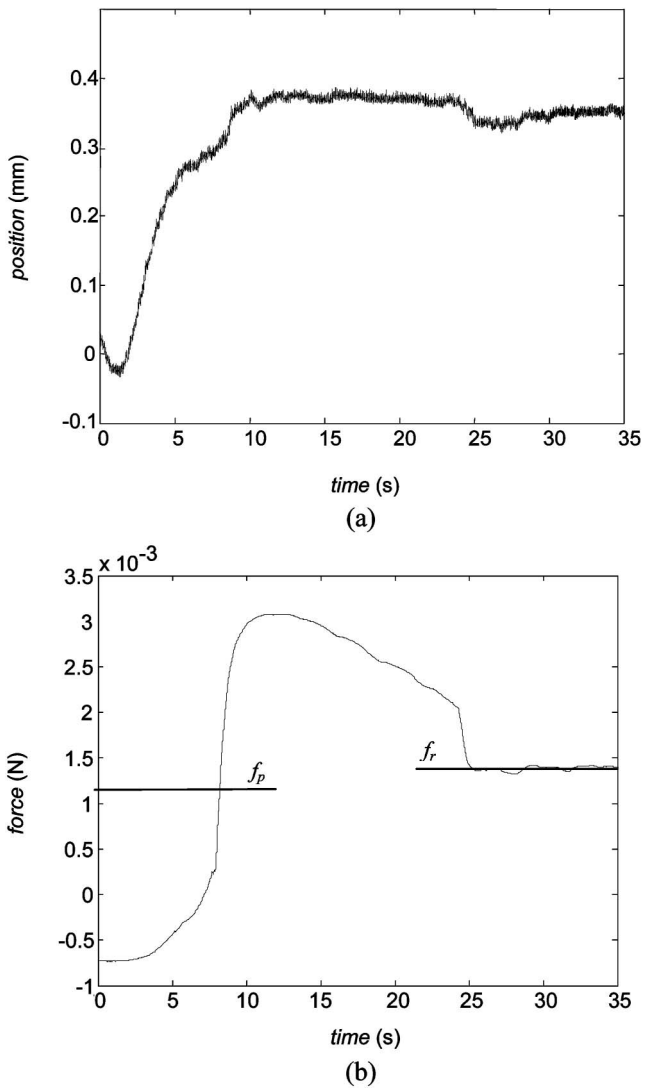

Fig. 10 (a) Actual position profile and (b) the actual force profile generated by the IPMC actuator under the hybrid control. The laser distance sensor and the precision load cell recorded these two profiles simultaneously

to 3.22 s. The phase margin of the position controller was 71.7° and the crossover frequency was 2.2 Hz. After implementing this position controller, the overshoot was reduced to 20.3 per cent and the settling time to 2.56 s.

The microscale precision force and position control capability of an IPMC has been demonstrated in this paper. The force resolution was 8 μN with a force noise of 0.5 μN r.m.s. The position resolution was 6 μm with a position noise of 2.5 μm r.m.s. The maximum force and tip displacement achieved with the IPMC actuator under closed-loop control were 2 mN and 5 mm respectively. The IPMC actuator tracked sinusoidal and trapezoidal force and position trajectories well under closed-loop control. The maximum velocity that the IPMC actuator could generate was 3 mm/s.

A novel hybrid control strategy was successfully implemented on the IPMC actuator system. It experimentally demonstrated an effective switching mechanism between the position and force control loops when the sensed force exceeded a predetermined threshold. The proposed hybrid position and force control scheme showed great potential in practical applications such as a robotic microgripper for effective manipulation of a delicate object without damaging it.

ACKNOWLEDGEMENTS

The authors are grateful to Dr Donald Leo and Mr Matt Bennett of Virginia Polytechnic Institute and State University for their generosity in providing IPMC samples.

REFERENCES

1 **Bar-Cohen, Y.** *Electroactive Polymer* (*EAP*) *Actuators as Artificial Muscles*, 2001, SPIE publication, Ch. 1 (Society of Photo-optical Instrumentation Engineers, Bellingham, Washington).

2 **Shahinpoor, M., Bar-Cohen, Y., Simpson, J. O.** and **Smith, J.** Ionic polymer–metal composites (IPMCs) as biomimetic sensors, actuators and artificial muscles—a review. *Int. J. Smart Mater. Structs*, 1998, **7**, R15–R30.

3 **Shahinpoor, M.** Conceptual design, kinematics and dynamics of swimming robotic structures using ionic polymeric gel muscles. *Int. J. Smart Mater. Structs*, 1992, **1**, 91–94.

4 **Oguru, K., Kawami, Y.** and **Takenaka, H.** Bending of an ion-conducting polymer film-electrode composite by an electric stimulus at low voltage. *Trans. J. Micromach. Soc.*, 1992, **5**, 27–30.

5 **Sadeghipour, K., Salomon, R.** and **Neogi, S.** Development of a novel electrochemically active membrane and 'smart' material based vibration sensor/damper. *Int. J. Smart Mater. Structs*, 1992, **1**, 172–179.

6 **Hunter, I.** and **Lafontaine, S.** A comparison of muscle with artificial actuators. In *Technical Digest of the IEEE Solid State Sensor and Actuator Workshop*, 1992, pp. 178–185.

7 **Konyo, M., Tadokoro, S., Takamori, T.** and **Oguru, K.** Artificial tactile feel display using soft gel actuators. In Proceedings of IEEE International Conference on *Robotics and Automation*, April 2000, pp. 3416–3421.

8 **Bar-Cohen, Y., Leary, S., Yavrouian, A., Oguru, K., Tadokoro, S., Harrison, J., Smith, J.** and **Su, J.** Challenges to the application of IPMC as actuators of planetary mechanisms. In Proceedings of SPIE Symposium on *Smart Structures and Materials*, March 2000, Vol. 3987, paper 21.

9 **Bar-Cohen, Y., Xue, T., Shahinpoor, M., Simpson, J. O.** and **Smith, J.** Flexible, low-mass robotic arm actuated by electroactive polymers and operated equivalently to human arm and hand. In Proceedings of ASCE *Robotics 98*, April 1998, pp. 15–21.

10 **Shahinpoor, M.** Continuum electromechanics of ionic polymeric gels as artificial muscles for robotic applications. *Smart Mater. Structs*, 1994, **3**, 367–372.

11 **Lumia, R.** and **Shahinpoor, M.** Microgripper design using electroactive polymers. In Proceedings of SPIE Symposium on *Smart Structures and Materials*, March 1999, Vol. 3669, pp. 322–330.

12 **Kim, W.-J.** and **Bhat, N.** Microgripper. Disclosure of Invention 1868TEES02, Texas A&M University System, February 2002.

13 **Bhat, N.** and **Kim, W.-J.** Precision control of force produced by ionic polymer metal composite. Accepted for presentation in 2003 ASME International Mechanical Engineering Congress and Exposition, November 2003.

14 Baumer Electric. Measuring at an angle with the OADM 20144xx and OADM20145xx.

15 **Mallavarapu, K.** Feedback control of ionic polymer actuators. Master's thesis, Virginia Polytechnic Institute and State University, July 2001.

16 **Kothera, C.** Micro-manipulation and bandwidth characterization of ionic polymer actuators. Master's thesis, Virginia Polytechnic Institute and State University, December 2002.

17 **Richardson, R., Levesley, M. C., Brown, M. D., Hawkes, J. A, Watterson, K.** and **Walker, P. G.** Control of ionic polymer metal composites. *IEEE/ASME Trans. Mechatronics*, 2003, **8**(2), 245–253.

18 **Kanno, R., Kurata, A., Hattori, M., Tadokoro, S., Takamori, T.** and **Oguro, K.** Characteristics and modeling of ICPF actuator. In Proceedings of Japan–USA Symposium on *Flexible Automation*, July 1994, Vol. 2, pp. 691–698.

19 *Optimization Toolbox* (The Mathworks, Inc., Natick, Massachusetts).

mi00001003 04-08-04 16:40:13 Rev 14.05
The Charlesworth Group, Huddersfield 01484 517077